Electrical characteristics of light-emitting electrochemical cells based on a wide bandgap polymer

M. Sampietro and R. Sotgiu
Politecnico di Milano, Dipartimento di Elettronica e Informazione, Piazza Leonardo da Vinci 32, 20133 Milano, Italy

F. P. Wenzl, L. Holzer, S. Tasch, and G. Leising
Institut für Festkörperphysik, Technische Universität Graz, Petersgasse 16, A-8010 Graz, Austria
(Received 22 January 1999; revised manuscript received 16 July 1999)

We report on the electrical characteristics of light-emitting electrochemical cells based on a methyl substituted ladder-type poly(paraphenylene) (*m*-LPPP). Current-voltage (*I*-*V*) characteristics and capacitance-voltage (*C*-*V*) plots are used to track the formation of the highly conductive contacts, the initial diffusive carrier transport regime, the onset of a net voltage drop across the polymeric bulk, and the final resistive behavior of the device in which carriers are mostly driven by drift. The analysis of the *C*-*V* plots reveals a strong increase of the capacitance at the threshold as a signature of the large carrier injection through the contacts and their diffusion through the active layer. From the physical analysis of the device behavior an electrical model is drawn.

I. INTRODUCTION

Light-emitting electrochemical cells[1–10] (LEC's) are experiencing increasing scientific and industrial interest as solid-state sources of luminescence, thanks to their good electroluminescence efficiency, low driving voltages, and ease of fabrication. As introduced by Pei *et al.*,[1] a LEC consists of a polymer blend embedded in between two electrodes, at least one of the two being transparent [typically indium tin oxide (ITO)]. The polymeric blend is comprised of a luminescent polymer, a salt (typically lithium triflate) and an ion conducting polymer [typically poly(ethylene-oxide)-PEO] in which the salt dissolves to form ions.[11,12] This composition determines the difference between LEC's and polymer light-emitting diodes (LED's).[13] In a LED the active layer consists of the pristine electroluminescent polymer and the electrical characteristics are inevitably dependent on the nature of the interfaces between the polymer and the electrodes (relative work functions of the two electrode materials,[14] use of charge transport layers,[15,16] interface traps[17]). Therefore the LED's, especially the ones based on wide band-gap polymers,[18] are characterized by high turn on voltages, that have to be reduced for the successful application of conjugated polymers in flat panel displays.

LEC's overcome that problem since low onset voltages, fairly independent of the potential barrier height at the interfaces polymer/electrodes, can be achieved due to the presence of mobile ions in the active layer, which strongly facilitate charge injection already at low applied voltages. We present a range of experimental measurements that extend the analysis already performed on LEC's (Refs. 2 and 9) and lead to a thorough investigation of the carrier transport phenomena in LEC's based on a wide band-gap polymer and allows us to draw a simple equivalent electric model for the device characteristics.

II. EXPERIMENT

The synthesis of *m*-LPPP is reported in Refs. 19 and 20. Poly(ethylene oxide), MW 5 000 000, and lithium triflate ($LiCF_3SO_3$) were purchased from Aldrich Corp. and were heated under high vacuum to remove any content of water before use. The LEC's were produced by spin coating a solution of *m*-LPPP, PEO, and $LiCF_3SO_3$, in a weight ratio of 20:10:3, in cyclohexanone on an ITO coated glass substrate (film thickness$\approx$200 nm). The films were heated afterwards at $T=60\,^{\circ}\mathrm{C}$ under argon atmosphere to remove any content of solvent. Afterwards aluminum was evaporated as a top electrode (thickness$\approx$50 nm).

Current-voltage measurements have been performed with a HP4142B modular source/monitor instrument at slow voltage scanning, while for the capacitance-voltage measurements a HP4274A LCR meter was used. All measurements were performed at room temperature and under argon atmosphere.

III. BASIC CHARACTERISTICS OF LEC's BASED ON *m*-LPPP

We have recently presented the characteristics of *m*-LPPP based LEC's.[21,22] The devices turn on at about 2.7 V when ITO and Al are used as the electrodes. This value matches very well with the single particle energy gap of *m*-LPPP divided by the elementary charge *e*. The electroluminescence (EL) efficiency was found to be similar to that of *m*-LPPP based LED's, but the turn on occurs at much lower voltages than for LED's of comparable thickness based on pure *m*-LPPP.

Differently from other LEC's reported up to now, our LEC's based on *m*-LPPP showed an asymmetric behavior in their EL-*V* characteristics (and partially also in their *I*-*V* characteristics),[21,22] that is they turn on at low voltages only when ITO is contacted as a cathode (generally referred to as reverse direction in LED's), but not in forward direction. The origin of this unexpected behavior can be explained by analyzing the distribution of the ions within the active layer of the LEC. The distribution of ions was probed by secondary-ion-mass spectroscopy (SIMS), which reveals that the lithium triflate ions are already spatially separated after fabrication, with the Li^+ ions anchored near the ITO electrode,

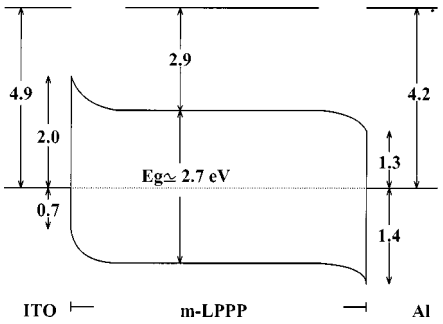

FIG. 1. Energy-band diagram at equilibrium of a LEC based on *m*-LPPP with ITO and aluminum contacts. The Fermi level of the intrinisic *m*-LPPP is assumed to be around mid gap.

whereas the triflate$^-$ ions are mobile.[23–25] In this case *n*-type doping of *m*-LPPP will only be possible using ITO as the cathode (*reverse* bias). Note that for the reverse biasing direction the charge carrier injection is supposed to be more difficult, since the nominal potential barriers at the interfaces polymer/electrodes are increased compared to the forward bias direction. Therefore, although our *m*-LPPP based LEC's do not show the symmetric characteristic *I-V* and *EL-V* curves expected for LEC's, the working principle of these devices is totally different from LED's.

The energy-band diagram of a short circuit LEC based on *m*-LPPP at equilibrium is shown in Fig. 1. The drawing highlights the large energy barriers (≈1.4 eV and ≈2 eV) the charge carriers have to overcome to be injected from the electrodes into the polymer. In thermal equilibrium, the internal built-in field is screened in the bulk of the layer and the built-in voltage hence drops at the interfaces polymer/electrodes (compare also with Ref. 7).

IV. ELECTRICAL CHARACTERISTICS OF REVERSE BIASED LEC

Figure 2 shows the small signal capacitance measured on the device in forward bias (positive voltage to ITO) and in reverse bias (positive voltage on aluminum). Largely more pronounced than in the *I-V* characteristics (see Refs. 21 and 22), a strong asymmetry in the *C-V* plot is visible. Whereas the capacitance in reverse direction strongly increases above a threshold voltage, the capacitance in forward direction is

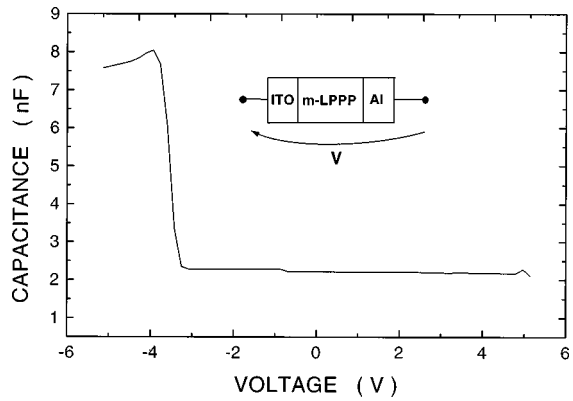

FIG. 2. Capacitance behavior of the *m*-LPPP LEC as a function of the external applied voltage (forward and reverse bias). The device sketch shows positive versus the applied voltage.

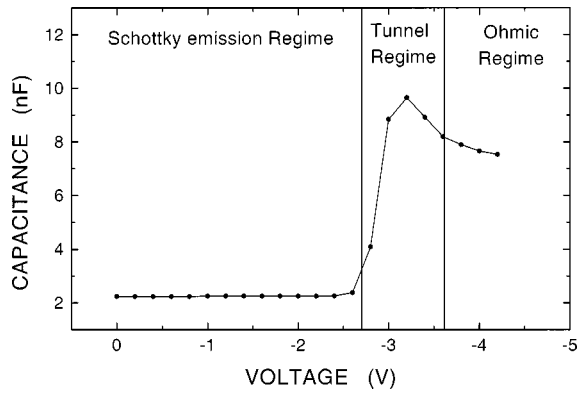

FIG. 3. Small signal capacitance of a *m*-LPPP LEC in reverse bias. Capacitance has been measured at a frequency of 10 kHz. The figure highlights the three transport regimes in the device depending on the applied reverse voltage.

almost voltage independent. The reason for that can be found in the above-mentioned restricted motion of ions in the *m*-LPPP LEC's: since the Li^+ seems to be anchored to the ITO bottom electrode independent of the applied voltage, only a reverse bias ensures Li^+ and triflate$^-$ ions to separate and to distribute on the two sides of the device, close to the ITO and aluminum contacts, respectively. In the following paragraphs we therefore will only discuss the reverse direction of these LEC's in which light emission occurs.

Figure 3 is an expanded view of the reverse bias section of the *C-V* measurement of a *m*-LPPP LEC, while Fig. 4 is the (a) linear and (b) logarithmic plot of the current measure-

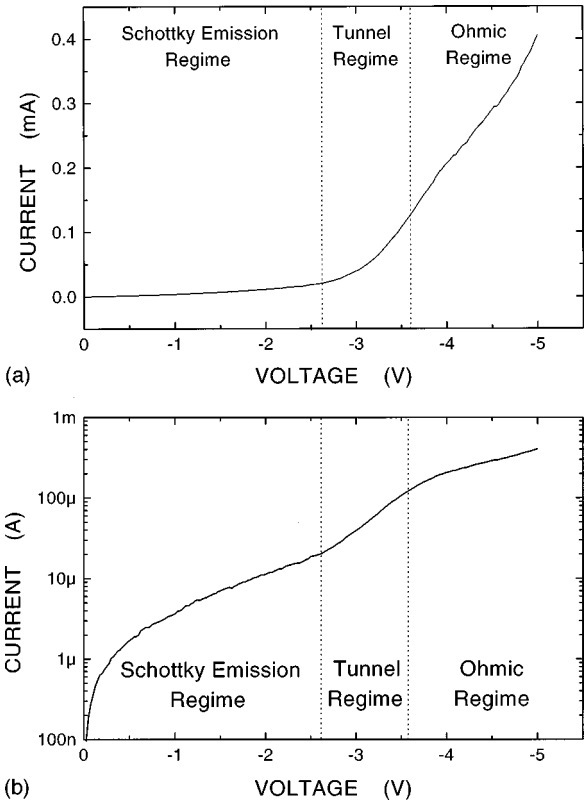

FIG. 4. (a) Current measurement in reverse bias of a *m*-LPPP LEC and (b) its logarithmic plot.

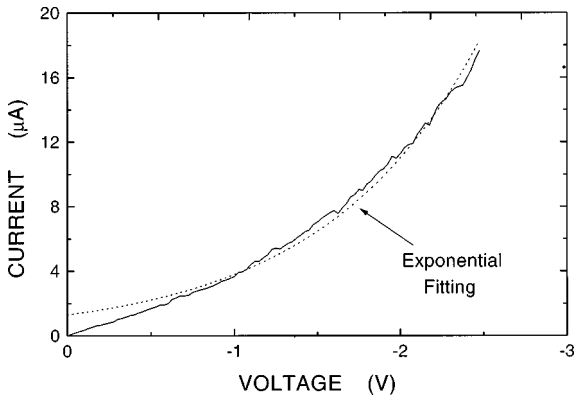

FIG. 5. Experimental data and exponential fitting of the *I-V* curve of Fig. 4 below threshold.

ment. One has to keep in mind that any slight change in the concentration ratios, preparation conditions, and area of the LEC's will influence these absolute values (current densities, geometric capacitance, bulk resistance) depicted in that graphs but not the basic electrical characteristics of the LEC's, which are described below.

A. Operation below threshold

The high potential barriers (see Fig. 1) at the interfaces between the conductive electrodes and the polymer prevent charge carriers to be injected into the polymer bulk in large quantity and justify the very low current level measured for small applied reverse voltages up to about 2.7 V. The injection of carriers through the barrier as a tunneling effect is excluded because the Fermi levels of the conductive electrodes are within the polymer energy gap (the Fermi level of ITO is below the lowest unoccupied molecular orbital (LUMO) level of the polymer and the Fermi level of Al is above the highest occupied molecular orbital (HOMO) level of the polymer). By expanding the current plot of Fig. 4 below threshold, a close to exponential behavior is seen (Fig. 5). This can be well explained by the lowering of the barrier height seen by charge carriers in their emission from the conductive electrodes to the polymer when an electric field is applied. The dependence corresponds to an effect that was explained many years ago by Walter Schottky when electron emission into vacuum was studied. For this reason the barrier lowering is indicated as ''Shottky effect'' in literature[26] and is schematically reported in Fig. 6. The effective barrier $q\Phi_B$ is lowered by the combined effect of the electric field and of the image charge force. By fitting the experimental data with an exponential curve and comparing it with the expression for thermionic injection from the conductor to the polymer, we can estimate the effective barrier lowering $\Delta\Phi(V)$:

$$J = A \cdot \exp\left(- \frac{q[\Phi_B - \Delta\Phi(V)]}{kT} \right), \tag{1}$$

where k is the Boltzmann constant and T the absolute temperature. This results to be $\Delta\Phi(V) \cong 16$ meV for every volt applied to the LEC. This value is a little larger than what is found in inorganic metal-semiconductor junctions, because in the case of LEC the barrier lowering effect is enhanced by

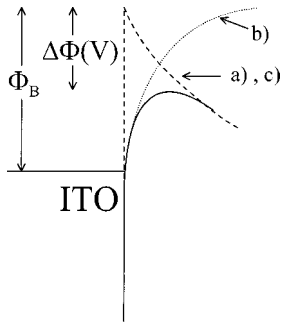

FIG. 6. Schematic of the lowering of the potential energy barrier between the conductive electrode (ITO) and the polymer. The effective barrier Φ_B is lowered by $\Delta\Phi$ because of the combined effect of the applied electric field (a), of the image charge (b), and of the accumulation of mobile ions at the contact (c), this latter being a peculiarity of the LEC.

the presence of mobile ions that tend to concentrate the electric field at the interface. Indeed, as the applied external voltage is increased, the electric field drives the mobile ions (positive and negative) towards the side contacts. As pointed out in Refs. 7 and 9, the ions concentrate at the two interfaces and redistribute the electric field away from the bulk of the device towards the interfaces and leaves only a very small finite electric field across the bulk of the polymer layer. This effect can be visualized in the energy-band diagram of the device by a strong bending of the potential energy near the contacts, as shown in Fig. 7(a) for the case of an external voltage almost equal to *Eg*. The density of the ions close to the electrodes increases by increasing the external voltage

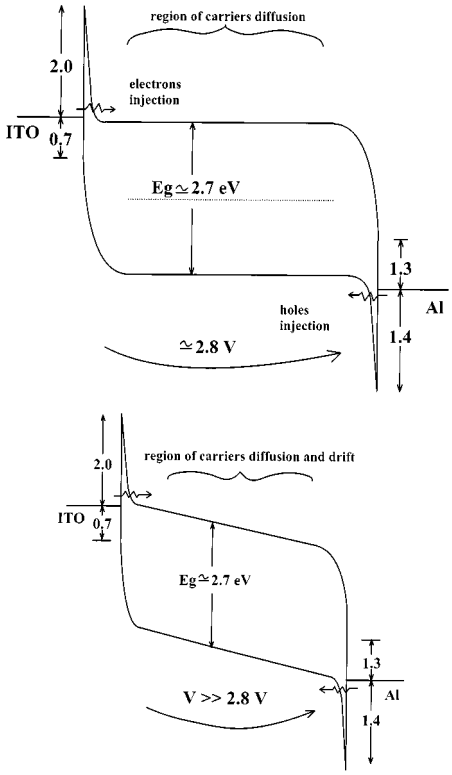

FIG. 7. Schematic energy-band diagrams of the LEC based on *m*-LPPP (a) biased around the threshold and (b) biased well above the threshold.

together with the local electric field, so that the width of the potential barrier at the interface is steadily decreased.

B. Strong carrier injection at the threshold

In the regime between 2.7 and 3.6 V the current increases rapidly with applied voltage. For voltages above 2.7 V the energy levels of the electrodes are higher in potential than the conduction and valence bands of the bulk material and the barrier width is already so thin that carrier injection becomes important and can be well described by a field induced tunneling process,[14] which follows the equation[26]

$$I=\frac{A^*T^2}{\Phi}\left(\frac{qE}{kT}\right)^2 e^{-2\gamma\Phi^{2/3}/3qE}, \tag{2}$$

where E is the electric field, and γ is a parameter which depends on the shape of the barrier, A^* material parameter, and Φ the potential barrier height. (This fast increase in current can hardly be attributed to a drifting mechanism in the LEC since the mobility of the charge carriers in *m*-LPPP is only weakly field dependent in that regime.[27]) Figure 1 shows that one can expect rather high values for Φ at both interfaces polymer/electrodes, in the range of 2 and 1.4 eV, respectively. Since in the low-voltage regime the whole external voltage drops across the ion accumulation zone at the interfaces, one can estimate an effective electric field at the interfaces equal to

$$E=V/2d_B, \tag{3}$$

where d_B is the width of ion accumulation zone at the interface and has been assumed to be symmetric at both interfaces in a first approximation. Since the values for Φ are comparably high, the current flow around the threshold can only be explained if the width of the potential barrier d_B is rather small, so that high electric fields are present at the interfaces, which generate effective charge-carrier injection according to Eq. (2).

The exponent of Eq. (2) can be determined by fitting the equation to the I-V curve, so that d_B can be calculated by the fit, if Eq. (3) is inserted into Eq. (2) and the nominal values from Fig. 1 are inserted for Φ_B. Under that approximation a value for d_B in the range between 0.5 and 0.6 nm is obtained. This extremely low value for d_B fits quite well with that predicted by deMello *et al.*[9] As the carriers are injected, the concentrations gradients for each type of carrier (high concentration of electrons on the cathode side, where they are injected, and none on the anode side where electrons are swept away by the contact; high concentration of holes on the anode side and none on the cathode side) drive a diffusion current:

$$J=qD_n\frac{dn}{dx}+qD_p\frac{dp}{dx} \tag{4}$$

which depends on the gradient of the charge carriers and on the diffusion constants D_n and D_p of the two types of carriers (*n* denotes negatively charged polarons and *p* positively charged polarons).

In steady-state conditions, in which Eq. (4) applies, the strong increase of the injected charge with the external voltage, as given by Eq. (2), has another important consequence in addition to the mentioned increase of carrier concentration gradients along the device that give rise to the diffusive transport mechanism. The additional effect is related to the accumulation of charge into the bulk of the device produced by the external voltage variation. For the sake of simplicity, consider a linear gradient distribution of one of the two carriers within the polymer in the shape of a triangle. By increasing the external voltage, the height of the triangle in the injecting side increases while the concentration of the same carriers at the collecting interface does not change. This has two consequences: the first is that the gradient increases, and this is mirrored in the increase of the steady-state current flowing along the device, as measured in Fig. 4. The second consequence is that the area increases, and there is an accumulation of carriers within the device. This effect is indeed an increase of charge deposited into the device as a consequence of an increase of external voltage, and therefore manifest itself as a capacitive behavior. By performing a C-V measurement, we very neatly mirror this effect, as can be seen by the experimental plot of Fig. 3. When the threshold is reached, the small signal capacitance undergoes a fast increase and gives a well precise signature of the threshold itself. This capacitive effect is typical of devices in which the carrier transport mechanism is diffusion and is therefore called ''diffusion capacitance.''[26,29] The diffusion capacitance adds to the geometrical capacitance of the device (Fig. 3 gives $C_{\text{geom}}\cong 2.2$ nF) and shows up for external voltages exceeding 2.7 V. The C-V measurement is performed by biasing the LEC to a given voltage and superposing a small voltage signal (of about 50 mV amplitude and 10 kHz frequency in our case) and measuring the current signal at 90° out of phase. The ratio of the two quantities leads to the capacitance value at that biasing voltage. The procedure is repeated for each bias voltage.

C. High-voltage operation

For applied voltages above the electrochemical redox potential, a *p* and *n* doping of the polymer near the interfaces will occur due to the interaction of the charge injected on the polymer chain and the surrounding ions. This doping can be evidenced by a strong polaronic absorption feature in the absorption spectrum of the LEC operated at these voltages, which occurs at an energetic position typical for doping in *m*-LPPP.[28] As soon as this electrochemical doping occurs, the electric field will not be screened anymore in the small area close to the interfaces since the doped polymer together with the ion form neutral species. A *p* and a *n* doped zone are therefore generated adjacent to the electrodes with an insulating layer in the middle, where the applied electric field mainly drops [see Fig. 5(b)], so that a *p*-*i*-*n* junction comes into existence. A theoretical description of that scenario is presented in Ref. 7. By referring to the energy diagram of

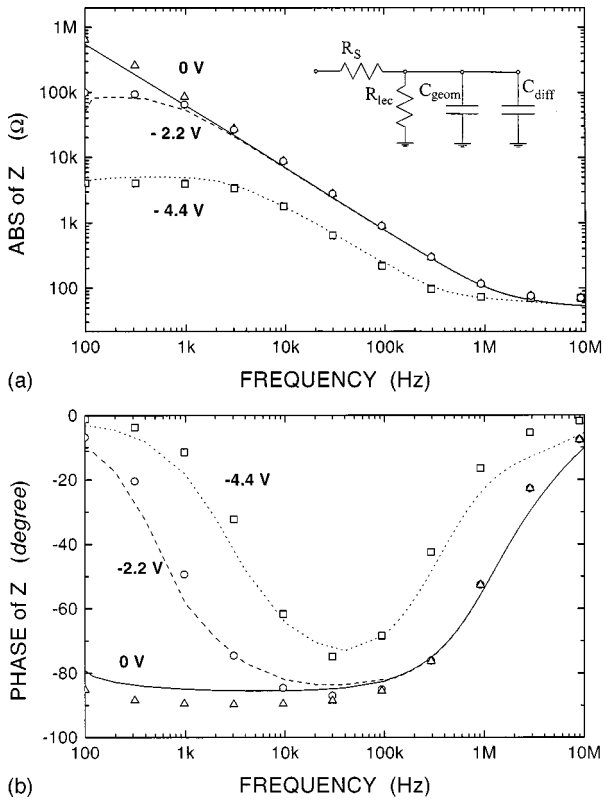

FIG. 8. Measured absolute value (above) and phase (below) behavior of the LEC impedance as a function of the frequency for three different applied voltages. In the inset is the circuit model of the device. The dotted line is obtained by simulating the model with the following values for the components: For $V=0$ V: $R_{\mathrm{LEC}}=20\ \mathrm{M}\Omega$, $C_{\mathrm{diff}}=0$ nF, $R_S=80\ \Omega$, $C_{\mathrm{geom}}=2.2$ nF; for $V=-2.2$ V: $R_{\mathrm{LEC}}=100\ \mathrm{k}\Omega$, $C_{\mathrm{diff}}=0$ nF, $R_S=80\ \Omega$, $C_{\mathrm{geom}}=2.2$ nF; for $V=-4.4$ V: $R_{\mathrm{LEC}}=5\ \mathrm{k}\Omega$, $C_{\mathrm{diff}}=6.5$ nF, $R_S=80\ \Omega$, $C_{\mathrm{geom}}=2.2$ nF.

Fig. 7(b), we may consider the barrier for the carrier injection so thin that tunneling from the contacts into the polymer is freely possible (Ohmic contacts) and that the additional voltage applied to the device necessarily drops across the bulk layer.

The effect of this electric field is that the current flow through the LEC is no longer governed only by carrier diffusion but also has a drift component that increases as the external voltage is increased. Since it is mainly due to drift of charge carriers, the *I-V* characteristic of the LEC based on *m*-LPPP above 3.5 V [see Fig. 3(b)] shows an Ohmic behavior, which is limited by the internal resistance of the more or less insulating undoped bulk polymer ($R\approx 5\ \mathrm{k}\Omega$).

V. LEC MODEL WITH IMPEDANCE MEASUREMENTS

The different regimes of operation of the LEC and the onset of a dominant diffusion capacitance above threshold are well mirrored in the impedance measurements, as shown in Fig. 8(a) (absolute value) and Fig. 8(b) (phase relationship). The insert in the figure is a circuit model of the LEC based on the physical characteristics of the device as highlighted in the previous paragraphs: R_S is a series resistance due to the contacts between the wires and the electrodes. Its value has been measured to be about 80 Ω due to the high resistance-per-square of the ITO electrode; C_{geom} is the geometrical capacitance of the device, measured to be 2.2 nF from Fig. 3; R_{LEC} is the internal resistance of the LEC and C_{diff} is its diffusion capacitance.

Well below the threshold (curves indicated with ''0 V'' in the figures), the device behaves like a capacitor, whose value is almost purely given by geometrical considerations and therefore equal to C_{geom}. The linear dependence of the absolute value of the impedance on the frequency in the low-frequency range certify that the internal resistance R_{LEC} of the device is higher than 10 MΩ.

The reduction of the internal resistance when carrier injection takes place is quantitatively reflected in the graphs by the flat behavior of the absolute value at low frequencies [Fig. 8(a)] and by a corresponding angle shift in the phase plot [Fig. 8(b)]. At very weak injection ($V=2.2$ V) the value of $R_{\mathrm{LEC}}=100\ \mathrm{k}\Omega$ can be, for example, calculated.

Well above the threshold ($V=4.4$ V), the internal resistance drops down to $R_{\mathrm{LEC}}\cong 5\ \mathrm{k}\Omega$ and, with reference to the circuit model in the inset, the diffusion capacitance can be extracted from the measurements to be about 6.5 nF, in good agreement with the value obtained in the *C-V* plot of Fig. 3. The onset of this capacitance, which adds to C_{geom}, is responsible of the shift to the left of the phase curve at high frequency [Fig. 8(b)], while the lower value of R_{LEC} is responsible of the smaller phase angle at low frequencies.

The marked points in Figs. 8(a) and 8(b) are the values of impedance obtained from the model by using the mentioned values for the circuit elements. The good agreement with experiments leads to confidence to the physics that generated the model.

VI. CONCLUSIONS

The electrical characteristics of LEC's based on *m*-LPPP as a representative of high band-gap conjugated polymers have been analyzed. In dependence of the applied voltage three different regimes have been identified, which determine the working principle of these LEC's.

In the first regime the current flow is very low and determined by thermionic emission over a barrier whose height is lowered by Schottky effect. At higher applied voltages in the range of the optical band gap, the current flow through the LEC strongly increases due to field induced tunneling injection of charge carriers from the electrodes through the thin potential barrier at the interfaces into the active layer. A third, Ohmic regime is observed, if the applied voltage is increased above the electrochemical redox potential of the active conjugated polymer layer, where an electrochemical doping of the polymer occurs.

ACKNOWLEDGMENTS

We are indebted to U. Scherf and K. Müllen for denoting the *m*-LPPP powder. We gratefully acknowledge the financial support of the Italian MURST and CNR, and of the Sonderforschungsbereich Elektroaktive Stoffe and the TMR project EUROLED.

[1] Q. Pei, G. Yu, C. Zhang, Y. Yang, and A. J. Heeger, Science **269**, 1086 (1995).
[2] Q. Pei, Y. Yang, G. Yu, C. Zhang, and A. J. Heeger, J. Am. Chem. Soc. **118**, 3922 (1996).
[3] Y. Cao, G. Yu, Y. Yang, and A. J. Heeger, Appl. Phys. Lett. **68**, 3218 (1996).
[4] H. Campbell, D. L. Smith, C. J. Neef, and J. P. Ferraris, Appl. Phys. Lett. **72**, 2565 (1998).
[5] Y. F. Li, J. Gao, G. Yu, Y. Cao, and A. J. Heeger, Chem. Phys. Lett. **287**, 83 (1998).
[6] G. Yu, Y. Cao, C. Zhang, Y. F. Li, J. Gao, and A. J. Heeger, Appl. Phys. Lett. **73**, 111 (1998).
[7] D. L. Smith, J. Appl. Phys. **81**, 2869 (1997).
[8] I. Riess and D. Cahen, J. Appl. Phys. **82**, 3147 (1997).
[9] J. C. deMello, N. Tessler, S. C. Graham, and R. H. Friend, Phys. Rev. B **57**, 12 951 (1998).
[10] J. A. Manzanares, H. Reiss, and A. J. Heeger, J. Phys. Chem. B **102**, 4723 (1998).
[11] P. G. Bruce, Philos. Trans. R. Soc. London, Ser. A **354**, 415 (1996).
[12] P. G. Bruce and C. A. Vincent, J. Chem. Soc., Faraday Trans. **89**, 3187 (1993).
[13] J. H. Burroughes, D. D. C. Bradley, A. R. Brown, R. N. Marks, K. MacKay, R. H. Friend, P. L. Burn, and A. B. Holmes, Nature (London) **347**, 539 (1990).
[14] I. D. Parker, J. Appl. Phys. **75**, 1656 (1994).
[15] A. R. Brown, D. D. C. Bradley, J. H. Burroughes, R. H. Friend, N. C. Greenham, P. L. Burn, A. B. Holmes, and A. Kraft, Appl. Phys. Lett. **61**, 2793 (1992).
[16] C. W. Tang, S. A. VanSlyke, and C. H. Chen, J. Appl. Phys. **65**, 3610 (1989).
[17] E. Ettedgui, H. Razafitrimo, Y. Gao, and B. R. Hsieh, Appl. Phys. Lett. **67**, 2705 (1995).
[18] G. Grem, G. Leditzky, B. Ulrich, and G. Leising, Adv. Mater. **4**, 36 (1992).
[19] U. Scherf and K. Müllen, Makromol. Chem. **12**, 489 (1991).
[20] U. Scherf, A. Bohnen, and K. Müllen, Makromol. Chem. **193**, 1127 (1992).
[21] F. P. Wenzl, S. Tasch, J. Gao, L. Holzer, U. Scherf, A. J. Heeger, and G. Leising, in *Electrical, Optical, and Magnetic Properties of Organic Solid-State Materials IV*, edited by J. R. Reynolds, A. K.-Y. Jen, L. R. Dalton, M. F. Rubner, and L. Y. Chiang, MRS Symposia Proceedings No. 488 (Materials Research Society, Pittsburgh, 1998), p. 57.
[22] S. Tasch, J. Gao, F. P. Wenzl, L. Holzer, U. Scherf, K. Müllen, A. J. Heeger, and G. Leising, Electrochem. Solid-State Lett. **2**, 203 (1999).
[23] L. Holzer, F. P. Wenzl, R. Sotgiu, M. Gritsch, S. Tasch, H. Hutter, M. Sampietro, and G. Leising, Synth. Met. **102**, 1022 (1999).
[24] J. Gao, G. Yu, and A. J. Heeger, Appl. Phys. Lett. **71**, 1293 (1997).
[25] G. Yu, Y. Cao, M. Andersson, J. Gao, and A. J. Heeger, Adv. Mater. **10**, 385 (1998).
[26] S. M. Sze, *Physics of Semiconductor Devices* (Wiley, New York, 1995).
[27] D. Hertel, U. Scherf, and H. Bässler, Adv. Mater. **10**, 1119 (1998).
[28] F. P. Wenzl, M. Zagorska, A. Pron, and G. Leising (unpublished).
[29] R. Muller and T. Kamins, *Device Electronics for Integrated Circuits*, 2nd ed. (Wiley, New York, 1986).